

Article

A Family of Lanthanoid Dimers with Nitroanilato Bridges

Samia Benmansour ^{1,*}, Gustavo López-Martínez ¹, Josep Canet-Ferrer ^{1,2} and Carlos J. Gómez-García ^{1,*}

¹ Instituto de Ciencia Molecular (ICMol), Universidad de Valencia, C/Catedrático José Beltrán 2, 46980 Paterna, Spain; gustavo.lopez@uv.es (G.L.-M.); jose.canet-ferrer@uv.es (J.C.-F.)

² ICFO-Institut de Ciències Fotoniques, Barcelona Institute of Science and Technology, 08860 Castelldefels, Spain

* Correspondence: sam.ben@uv.es (S.B.); carlos.gomez@uv.es (C.J.G.-G.); Tel.: +34-96-354-4423 (S.B. & C.J.G.-G.); Fax: +34-96-354-3273 (S.B. & C.J.G.-G.)

Academic Editor: Núria Aliaga-Alcalde

Received: 11 August 2016; Accepted: 31 August 2016; Published: 6 September 2016

Abstract: The first complexes with lanthanoid ions and the nitroanilato ligand have been synthesized (nitroanilate dianion = $[\text{C}_6\text{O}_4(\text{NO}_2)_2]^{2-}$ = dianion of the 3,6-dinitro-2,5-dihydroxo-1,4-dibenzoquinone ligand). This family of dimers can be formulated as $[\text{Ln}_2(\text{C}_6\text{O}_4(\text{NO}_2)_2)_3(\text{H}_2\text{O})_{10}] \cdot 6\text{H}_2\text{O}$ with $\text{Ln}(\text{III}) = \text{Sm}$ (1), Gd (2), Tb (3), Dy (4), Ho (5), and Er (6). The X-ray structure of this family of isostructural complexes shows that they all present a dimeric structure where the Ln^{3+} ions are connected by a bis-bidentate nitroanilato ligand. Each metal completes its nonacoordination environment with a terminal bidentate nitroanilato ligand and five water molecules in a slightly distorted tri-capped trigonal prismatic geometry. The magnetic properties of this family show the expected contributions of the lanthanoid ions without any noticeable magnetic interaction through the nitroanilato ligand. The compounds present luminescence of the nitroanilato ligand superimposed with a weaker emission from the lanthanide ion in compound 5 (Ho).

Keywords: lanthanoid complexes; magnetic properties; luminescence properties; anilato-type ligands; nitroanilato

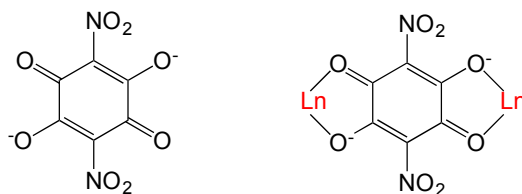
1. Introduction

The design and synthesis of polynuclear coordination complexes and coordination polymers with interesting physical properties is one of the hottest topics in Material Science nowadays. Thus, many coordination compounds have been synthesized with magnetic [1–3], electrical [4], and/or optical properties [5,6]. Another hot topic in the last decades has been the incorporation of two or more properties in the same compound. Thus, multi-functional materials combining electrical conductivity and ferromagnetism [7], superconductivity and magnetism [8], chirality and magnetism [9,10], or porosity and magnetism [11], have been reported in the last two decades.

Albeit, the design and synthesis of novel materials with tailored magnetic properties still remains a challenge. The most habitual strategies to reach this objective are: (i) using simple bridging ligands as cyanide (CN^-) [12], dicyanamide ($\text{N}(\text{CN})_2^-$) [13–15], azide (N_3^-) [16–20], oxalato ($\text{C}_2\text{O}_4^{2-}$) [21], ... combined with different transition metal atoms; (ii) using metalloligands, i.e., pre-formed metal complexes with vacant positions or labile ligands able to coordinate to other metal atoms [22–24] and (iii) using bridging ligands and co-ligands with different metal atoms to prepare coordination compounds with two or more different ligands and metals.

One of the most used ligands to prepare these coordination complexes and polymers is oxalato, since it can easily act as bis-bidentate bridging ligand connecting and coupling different magnetic

centers [21]. A topologically related family of ligands to oxalato is anilato and its derivatives ($C_6O_4X_2^{2-}$ = 3,6-disubstituted-2,5-dihydroxy-1,4-benzoquinone dianion, see Scheme 1). These ligands contain an aromatic ring replacing the central C=C skeleton of oxalato and can also act as bis-bidentate ligands coupling the metal centers they bridge [25].



Scheme 1. The nitroanilato ligand and its bis-bidentate coordination mode with Ln(III) ions.

Although all the aforementioned ligands have been mainly used with transition metal ions (especially with those of the first row), there is an increasing interest in the use of lanthanoid ions to prepare coordination complexes and polymers. This interest is due to the exceptional properties shown by these lanthanoid complexes in molecular magnetism [26–29]. An additional interest of lanthanoid-based coordination complexes is the presence of luminescence in many of them [30]. Thus, during the last decades, the photoluminescence properties of rare-earths have caught the attention of scientific community devoted to both fundamental and applied research [31–34]. The most attractive feature of luminescent lanthanoid compounds is related to their characteristic narrow emission lines [35,36]. Although photoluminescence of rare earths can be an efficient process, lanthanoid ions suffer from weak light absorption. Tailoring the rare earth environment by chemical synthesis is a key issue to overcome the problem of low absorption. This is the so-called antenna effect (or sensitization) [37–39]. The strategy consists of taking advantage of the intense absorption bands of organic chromophores to increase the carrier injection into the lanthanoid ion by intramolecular energy transfer. As possible ligands to play this role, we are currently exploring the family of anilato-type ligands of formula $(C_6O_4X_2)^{2-}$ with $X = H, Cl, Br, NO_2, \dots$

Using anilato-based ligands, we have recently prepared a family of heterometallic 2D honeycomb lattices formulated as $[M^{II}M^{III}(C_6O_4X_2)_3]^-$ with $M^{II} = Mn, Fe, \text{ and } Co$; $M^{III} = Cr \text{ and } Fe$ and $X = H, Cl, Br \text{ and } I$, where chirality and porosity coexist with tuneable long range magnetic order [1]. Interestingly, these 2D lattices are topologically identical to those obtained with lanthanoids, formulated as $[Ln_2(C_6O_4X_2)_3(H_2O)_6] \cdot nH_2O$ ($X = H \text{ and } Cl$) [40]. The main difference is the lack of planarity in the Ln(III) lattices since besides the three anilato ligands, each lanthanoid is coordinated by three water molecules in a tri-capped trigonal prismatic geometry. These layers have only been obtained with dhbq ($X = H$) and chloroanilato ($X = Cl$) but not with other anilato-derivatives. Since nitroanilato is a derivative that has never been used to prepare extended lattices with lanthanoids nor transition metals (except for a FeNa 2D lattice recently reported by some of us) [41], we have started a systematic study to try to prepare different complexes with lanthanoids and nitroanilato.

Remarkably, the nitroanilato ligand ($X = NO_2$) has been very scarcely used to prepare coordination compounds with any metal. In fact, a search in the CCDC database (updated February 2016), shows that there are only nine metallic complexes prepared with this ligand. Surprisingly, in all cases the metal ions are s-block metals as Na and K [42], or Ca and Sr [43], or d-block metals as Zn [44], Mo [45], Mn [46], Cr [47], and Fe [47]. Additionally, there is a very recent heterometallic 2D lattice where nitroanilato is coordinated to two different metals (Fe and Na) [41], but, as far as we know, no lanthanoid metal has ever been combined with this ligand.

Here we present the synthesis and characterization of the first complexes prepared with the ligand nitroanilato ($[C_6O_4(NO_2)_2]^{2-}$ = dianion of the 3,6-dinitro-2,5-dihydroxy-1,4-dibenzoquinone ligand, Scheme 1) and up to six different lanthanoid metal ions. These complexes can be formulated as $[Ln_2(C_6O_4(NO_2)_2)_3(H_2O)_{10}] \cdot 6H_2O$ with Ln(III) = Sm (1), Gd (2), Tb (3), Dy (4), Ho (5), and Er (6). All the

compounds are isostructural and consist of nitroanilato-bridged Ln(III) dimers. Here we present the single crystal X-ray structural characterization of 1–5 (the isostructurality of complex 6 was determined from X-ray powder diffraction, Figure S1) as well as their magnetic and luminescence properties.

2. Results and Discussion

2.1. Syntheses of the Complexes

The synthesis of the six compounds was performed under similar conditions using layering tubes to obtain good quality single crystals. The used metal:nitroanilato ratio (2:3) is the same found in the crystal structure of 1–5 and also in the family of anilato-based hetero-metallic 2D lattices formulated as $[\text{Ln}_2(\text{C}_6\text{O}_4\text{X}_2)_3] \cdot n\text{H}_2\text{O}$ [40], $A[M^{\text{II}}M^{\text{III}}(\text{C}_6\text{O}_4\text{X}_2)_3]$ [1] and $A_2[M^{\text{I}}M^{\text{III}}(\text{C}_6\text{O}_4\text{X}_2)_3]$ [48] ($A = [(\text{H}_3\text{O})(\text{phenazine})_3]^+$, NBu_4^+ , PBu_3Me^+ , PPh_3Et^+ or NBu_3Me^+ ; $M^{\text{I}} = \text{Na}$ or K ; $M^{\text{II}} = \text{Mn}$, or Fe ; $M^{\text{III}} = \text{Fe}$ and Cr ; $X = \text{H}$, Cl , Br or I). Albeit, when $X = \text{NO}_2$, these 2D lattices are not obtained but instead the series of Ln dimers 1–6 with a nitroanilato bridge are formed. Probably the larger steric hindrance of the NO_2 groups, that usually appear tilted ca. 30° – 50° with respect to the anilato ring [44,47], (as also observed in compounds 1–5, see below) is at the origin of this particular behavior.

2.2. Description of the Structures

Structure of $[\text{Ln}_2(\text{C}_6\text{O}_4(\text{NO}_2)_2)_3(\text{H}_2\text{O})_{10}] \cdot 6\text{H}_2\text{O}$ with Ln(III) = Sm (1), Gd (2), Tb (3), Dy (4), Ho (5), and Er (6). Compounds 1–6 are all isostructural and crystallize in the triclinic space group $P-1$ (Table 1). Compound 6 could not obtain as good quality single crystals and, therefore, its isostructurality has to be confirmed by X-ray power diffraction (see Figure S1 in Supplementary Materials).

Table 1. Crystal data and structure refinement of complexes 1–5.

	1	2	3	4	5
Formula	$\text{C}_{18}\text{H}_{32}\text{N}_6$ O_{40}Sm_2	$\text{C}_{18}\text{H}_{32}\text{N}_6$ O_{40}Gd_2	$\text{C}_{18}\text{H}_{32}\text{N}_6$ O_{40}Tb_2	$\text{C}_{18}\text{H}_{32}\text{N}_6$ O_{40}Dy_2	$\text{C}_{18}\text{H}_{32}\text{N}_6$ O_{40}Ho_2
F. Wt.	1273.20	1286.90	1290.31	1297.46	1302.32
Space group	$P-1$	$P-1$	$P-1$	$P-1$	$P-1$
Crystal system	Triclinic	Triclinic	Triclinic	Triclinic	Triclinic
a (Å)	8.0077(3)	8.0303(5)	8.0175(5)	7.9851(4)	8.0448(5)
b (Å)	10.7464(4)	10.7457(7)	10.7254(7)	10.6978(5)	10.7517(7)
c (Å)	12.1755(5)	12.1628(7)	12.1377(8)	12.1147(6)	12.1739(9)
α (°)	112.443(4)	112.596(6)	112.479(6)	112.273(5)	112.566(7)
β (°)	99.977(3)	100.577(5)	100.477(5)	100.339(4)	100.498(6)
γ (°)	101.730(3)	101.737(6)	101.785(5)	101.870(4)	101.758(5)
$V/\text{Å}^3$	911.01(7)	908.08(11)	904.28(11)	898.52(8)	911.62(12)
Z	1	1	1	1	1
T (K)	120	120	120	120	120
$\rho_{\text{calc}}/\text{g}\cdot\text{cm}^{-3}$	2.273	2.328	2.351	2.357	2.358
μ/mm^{-1}	3.340	3.770	4.030	4.277	4.458
$F(000)$	600	616	622	612	628
$R(\text{int})$	0.0439	0.0231	0.0273	0.0397	0.0211
θ range (deg)	2.91–25.04	2.82–25.04	2.91–25.04	2.92–25.07	2.82–25.04
Total reflections	9815	5886	5967	10448	6076
Unique reflections	3215	3213	3202	3180	3219
Data with $I > 2\sigma(I)$	2911	2989	2928	3041	3036
N_{var}	280	325	331	310	328
R_1^a on $I > 2\sigma(I)$	0.0392	0.0275	0.0285	0.0242	0.0279
wR_2^b (all)	0.0935	0.0578	0.0612	0.0597	0.0678
GOF ^c on F^2	1.076	1.056	1.048	1.081	1.082
$\Delta\rho_{\text{max}}$ ($\text{e}\text{Å}^{-3}$)	2.859	0.865	1.103	1.413	1.425
$\Delta\rho_{\text{min}}$ ($\text{e}\text{Å}^{-3}$)	−1.340	−0.596	−0.654	−0.685	−0.623

^a $R_1 = \sum ||F_o| - |F_c|| / \sum |F_o|$; ^b $wR_2 = [\sum w(F_o^2 - F_c^2)^2 / \sum w(F_o^2)^2]^{1/2}$; ^c GOF = $\sum [w(F_o^2 - F_c^2)^2 / (N_{\text{obs}} - N_{\text{var}})]^{1/2}$.

The structure consists of centrosymmetric dimers where the two lanthanoids are connected through a bis-bidentate nitroanilato ligand (Figure 1).

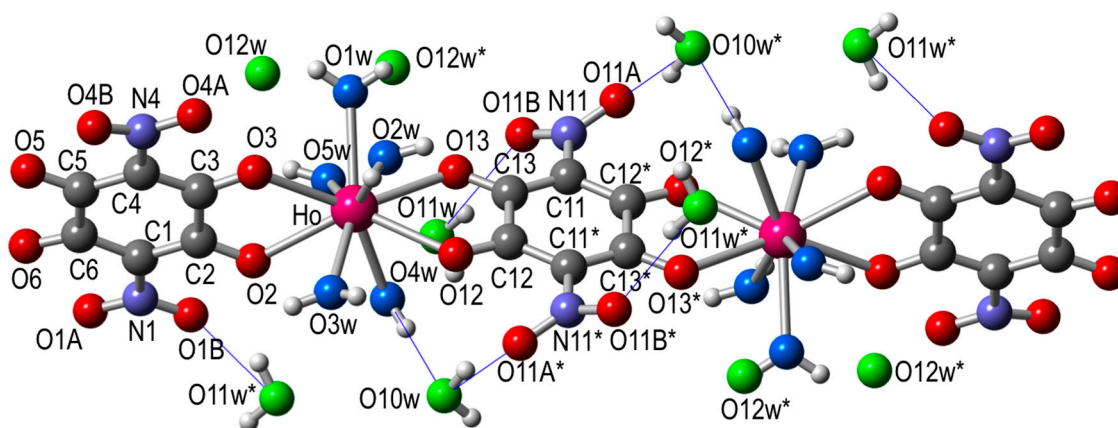


Figure 1. Structure of the dimer unit in $[\text{Ho}_2(\text{C}_6\text{O}_4(\text{NO}_2)_2)_3(\text{H}_2\text{O})_{10}] \cdot 6\text{H}_2\text{O}$ (**5**) showing the labelling scheme (same structure and labelling scheme for all the other compounds). Color code: Ho = pink, C = grey, O = red, coordinated O_w = light blue, crystallization O_w = green, N = dark blue, and H = white. Blue thin lines are the intermolecular H-bonds.

Each Ln(III) ion has a terminal bidentate nitroanilato ligand and completes its coordination environment with five coordinated water molecules. Therefore, the coordination environment of each Ln(III) ion is formed by four oxygen atoms from two nitroanilato ligands and five coordinated water molecules in a tricapped trigonal prismatic geometry (Figure 2). Each nitroanilato ligand occupies a basal position (one in the upper and one in the bottom triangles) and one of the capped positions of the lateral sides (Figure 2). The five water molecules occupy the remaining positions (four basal and a capped one).

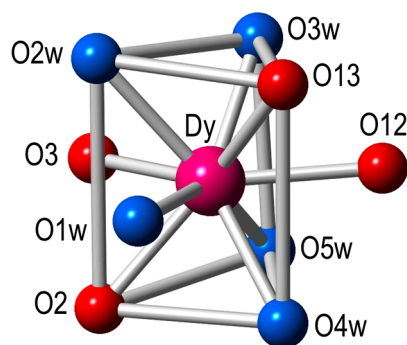


Figure 2. Coordination environment of the Dy(III) ion in the structure of **4** (same environment for all the other compounds). Color code: Dy = pink, O = red, O_w = light blue.

The dimers are located in layers parallel to the $[1,1,-1]$ plane (Figure 3) and show two types of intermolecular interactions: (i) π - π interactions between the aromatic rings of the terminal anilato ligands of two neighboring dimers and (ii) H-bonds connecting coordinated and crystallization water molecules with terminal oxygen atoms of the nitroanilato ligand (Table S1, Supplementary Materials and Figure 3).

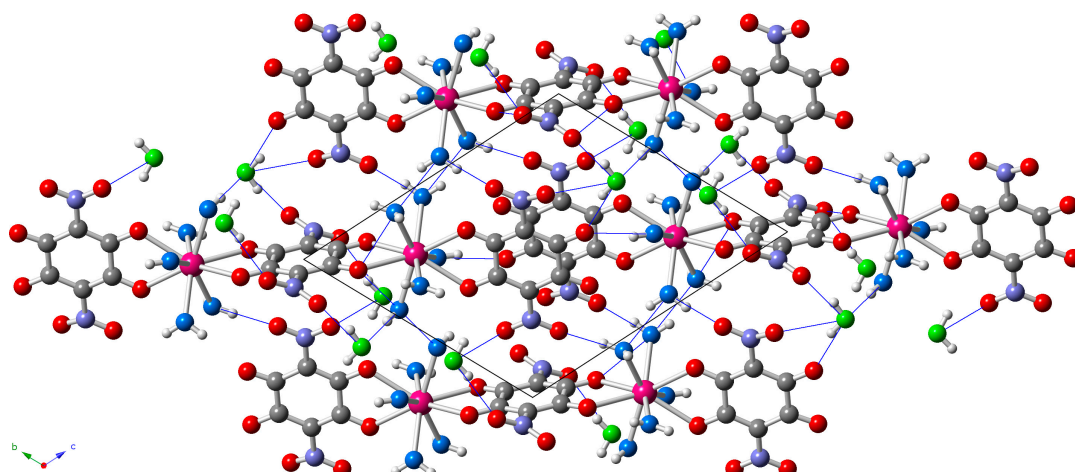


Figure 3. View of the layers parallel to the $[1,1,-1]$ plane in the structure of **5** showing the short intermolecular $O\cdots O$ distances as blue thin lines. Oxygen atoms of the coordination and crystallization water molecules are depicted in light blue and green, respectively.

A detailed analysis of the Ln–O bond distances (Figure 4, Table 2) shows that the Ln–O_{water} bond lengths are always shorter than the Ln–O_{NA} bond lengths of the nitroanilato ligand, as a consequence of the chelating coordination mode of nitroanilato. In all cases, the Ln–O_{NA} bond distances are longer for the bridging nitroanilato ligand (O12 and O13) than for the terminal one (O2 and O3). This fact agrees with the smaller electron density available in the oxygen atoms on the bridging ligand compared with the terminal ones. A remarkable fact observed in Figure 4 is the change shown by the Ho derivative in the expected decreasing trend in the bond distances as we move forward in the lanthanoids series. As a consequence of this increase in the Ln–O bond distances, the unit cell volume also shows an unexpected increase in the Ho derivative that breaks the decreasing trend observed in all the other derivatives (Figure 4, Table 2). This unexpected increase of all the Ln–O bond lengths in the Ho derivative is probably related with the lower distortion of its coordination polyhedron as confirmed by the sudden decrease of the dihedral angle of the average planes of the upper and lower triangular faces in the Ho complex (Figure 4).

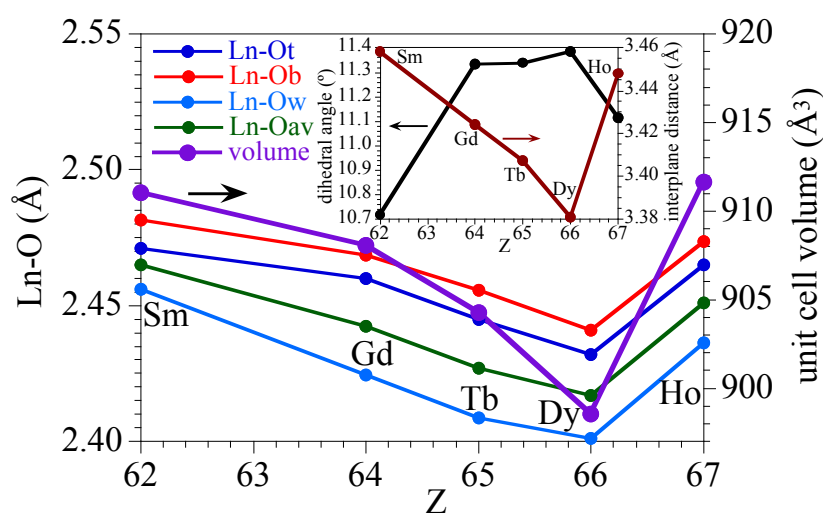


Figure 4. Variation of the Ln–O bond distances (terminal, bridging, water, and average, left scale) and the unit cell volume (right scale) for the series of compounds **1–5**. Inset shows the variation of the dihedral angle (left scale) and the distance (right scale) between the lower and upper triangular faces of the coordination polyhedron of the Ln(III) ion for the series of compounds **1–5**.

Table 2. Ln–O bond distances (Å), unit cell volume (Å³), and dihedral angle (θ) between the lower and upper triangular faces of the tricapped trigonal prismatic coordination polyhedron in compounds 1–5.

Atoms	Sm (1)	Gd (2)	Tb (3)	Dy (4)	Ho (5)
Ln–O2	2.490(4)	2.441(3)	2.420(3)	2.455(3)	2.482(3)
Ln–O3	2.453(4)	2.479(3)	2.470(3)	2.409(3)	2.448(3)
Ln–O12	2.480(5)	2.459(3)	2.450(3)	2.442(3)	2.466(3)
Ln–O13	2.483(4)	2.478(3)	2.461(3)	2.440(3)	2.481(3)
Ln–O1 _w	2.483(5)	2.429(3)	2.414(3)	2.403(3)	2.440(4)
Ln–O2 _w	2.459(5)	2.463(4)	2.434(3)	2.326(3)	2.464(4)
Ln–O3 _w	2.390(5)	2.433(3)	2.334(3)	2.421(3)	2.439(4)
Ln–O4 _w	2.480(5)	2.453(3)	2.411(4)	2.421(3)	2.367(4)
Ln–O5 _w	2.469(6)	2.345(3)	2.450(3)	2.435(3)	2.471(3)
Ln–O _{av}	2.465	2.442	2.427	2.417	2.451
V (Å ³)	911.01(7)	908.08(11)	904.28(11)	898.52(8)	911.62(12)
θ (°)	10.72	11.33	11.34	11.38	11.11

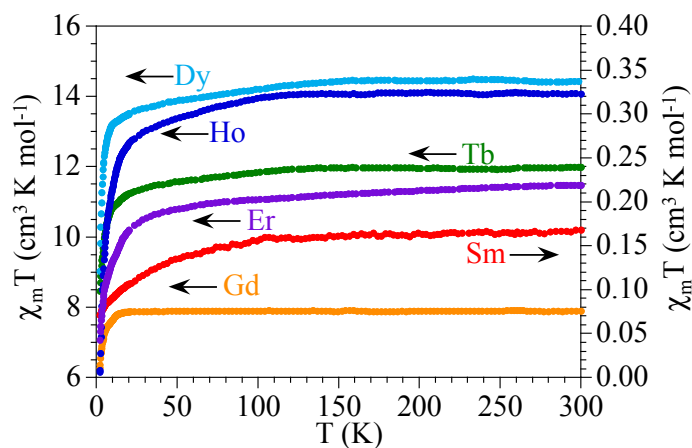
2.3. Magnetic Properties

The product of the magnetic susceptibility times the temperature ($\chi_m T$) per Ln(III) ion for the six compounds shows values of ca. 0.17, 7.9, 11.9, 14.3, 14.1, and 11.4 cm³·K·mol^{−1}, close to the expected ones (0.31, 7.87, 11.82, 14.17, 14.07, and 11.48 cm³·K·mol^{−1}, see Table 3) for isolated Sm(III), Gd(III), Tb(III), Dy(III), Ho(III), and Er(III) ions, respectively (Figure 5). When the temperature is decreased, all the compounds (except 2) show a soft decrease followed by a more pronounced one at lower temperatures to reach values of ca. 0.07, 8.5, 9.0, 6.2, and 7.1 cm³·K·mol^{−1} at 2 K for 1 and 3–6, respectively. The Gd derivative (compound 2) shows a constant value of $\chi_m T$ down to ca. 10 K where a more abrupt decrease appears to reach a value of ca. 6.3 cm³·K·mol^{−1} at 2 K (Figure 5).

Table 3. Relevant magnetic information for complexes 1–6.

Compound	Ln(III)	S	L	J	gJ ^a	$\chi_m T_{\text{calc}}$ ^b	$\chi_m T_{\text{exp}}$
1	Sm	5/2	5	5/2	2/7	0.09	0.08
2	Gd	7/2	0	7/2	2	7.87	7.9
3	Tb	3	3	6	3/2	11.82	11.9
4	Dy	5/2	5	15/2	4/3	14.17	14.3
5	Ho	2	6	8	5/4	14.07	14.1
6	Er	3/2	6	15/2	6/5	11.48	11.4

$$^a gJ = (3/2) \cdot [S(S+1) - L(L+1)] / [2J(J+1)]; \quad ^b \chi_m T_{\text{calc}} = (N_A g^2 \mu_B^2 / 3k) \cdot J(J+1).$$

**Figure 5.** Thermal variation of the $\chi_m T$ product per Ln(III) ion for the series of compounds 1–6.

The observed magnetic behavior in the six compounds are those expected for isolated or very weakly coupled Ln(III) ions [49]. The values observed at room temperature are close to those calculated for ${}^6\text{H}_{5/2}$, ${}^8\text{S}_{7/2}$, ${}^7\text{F}_6$, ${}^6\text{H}_{15/2}$, ${}^5\text{I}_8$, and ${}^4\text{I}_{15/2}$ ground multiplets for 1–6, respectively [50]. The decrease observed in all the samples expect in 2, is due to the progressive depopulation of the higher energy Stark components arising from the splitting of the aforementioned ground levels as a consequence of the ligand field. Of course, this decrease may also include a weak antiferromagnetic intradimer Ln-Ln coupling through the nitroanilato bridge. These results suggest that the nitroanilato ligand gives rise to very weak magnetic coupling. Note that although this weak coupling has been observed in other anilato-derivative ligands as chloroanilato and bromoanilato [1], it has never been observed before for nitroanilato since compounds 1–6 are the first magnetically characterized anilato-bridged complexes. Note that there are only two nitroanilato-bridged complexes with paramagnetic metals (Mo and Mn) reported to date, but none of them has been magnetically characterized [45,46].

2.4. Luminescence Properties

The luminescence of compounds containing the nitroanilato ligand is usually found around 500 nm in solution [51]. This emission varies after crystallization, resulting in a broad emission band centered at $\lambda_{\text{N}} = 596$ nm as shown in Figure 6a. The full width at the half maximum (FWHM) of this peak is about 85 nm estimated from the best Gaussian fit (in red). Importantly, this peak is also observed in our compounds, offering additional functionality to the system. For example, in the Ho(III) compound the ligand emission is clearly observed accompanied by additional radiative transitions, see Figure 6b. The best fitting shows, besides the ligand emission, two peaks centered at 541 and 643 nm (respectively noted as Ho1 and Ho2). Ho1 and Ho2 can be tentatively attributed to the well know radiative recombination channels at the Ho(III), ${}^5\text{F}_4 \rightarrow {}^5\text{I}_8$ and ${}^5\text{F}_5 \rightarrow {}^5\text{I}_8$, respectively [52]. These peaks show narrower FWHM, below 40 nm in the case of Ho2, as expected from rare earth emission. The integrated optical signal is around 30% of the total emitted light, which is an important rate having into account the high emission efficiency of the ligand.

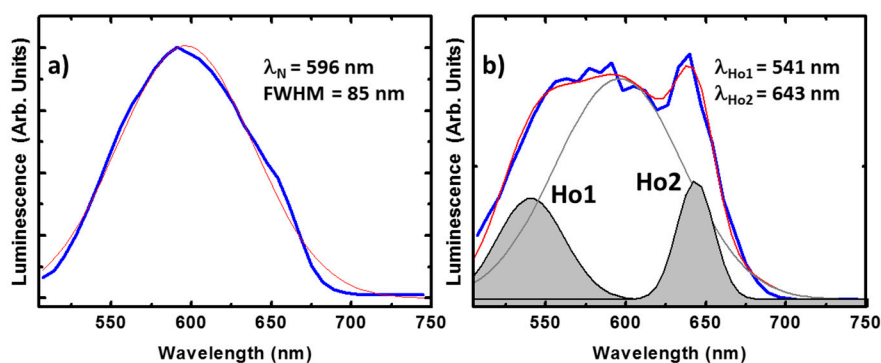


Figure 6. Emission spectra of the ligand (a) and the Ho(III) (b) compound. In both cases the spectrum corresponds to the average spectra in different points of single crystals excited at 405 nm wavelength. The experimental measurements are plotted in blue. The red curve is the best single and triple Gaussian fit, respectively. In the latter case, the contribution of the ligand is plotted in grey while the peak tentatively ascribed to the ion emissions are in black and shadowed.

For the Gd(III) and Er(III) compounds we cannot expect any contribution from the lanthanide ions. Quite particular is the case of the Gd(III) compound since the energy of the first excited state occurs at the ultra violet region. Thus, there are not available radiative recombination channels for Gd(III) ions at the visible range [53]. On the other hand, the optical activity of Er(III) compounds is centered at the near-infrared, because of the recombination from the first excited to the ground state (${}^4\text{I}_{13/2} \rightarrow {}^4\text{I}_{15/2}$). In these conditions, resonant optical pumping or up-conversion mechanisms must be employed for enabling visible light emission from the Er(III) ion, (e.g., via transitions such as ${}^4\text{S}_{3/2} \rightarrow$

$^4I_{15/2}$ or $^4F_{9/2} \rightarrow ^4I_{15/2}$). As a result, the corresponding luminescence spectra present minor differences with respect to the ligand crystal signal (Figure 7a,b): emission lines with $\text{FWHM}_{\text{Gd}} = 90$ nm and $\text{FWHM}_{\text{Er}} = 95$ nm centered around 590 nm.

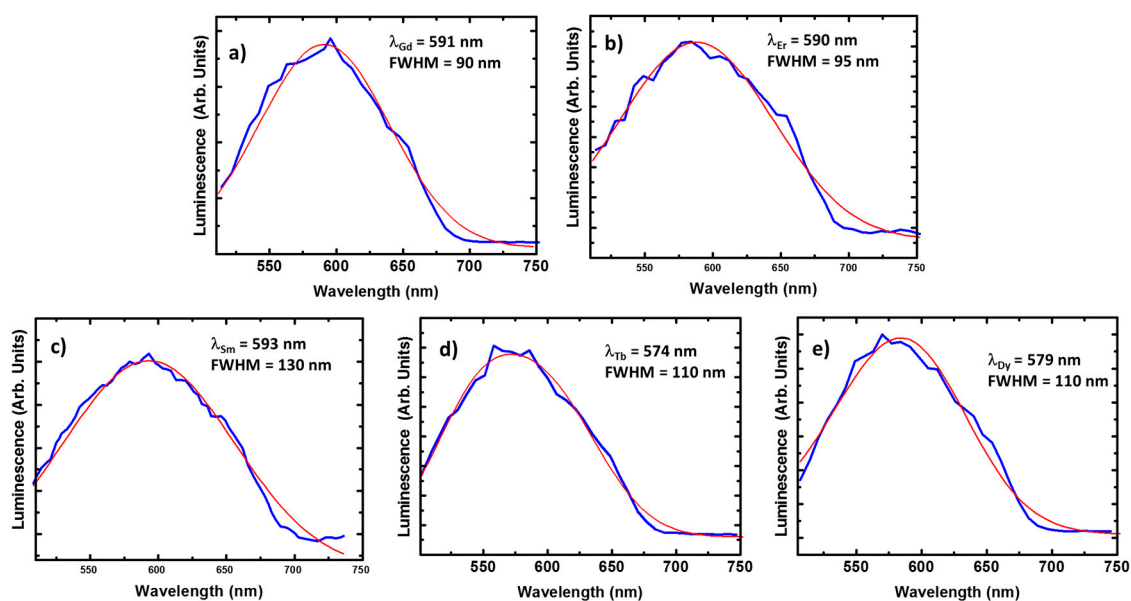


Figure 7. The emission spectra of the Gd(III) (a); Er(III) (b); Sm(III) (c); Tb(III) (d); and Dy(III) (e) compounds. The experimental data are plot in blue and the corresponding Gaussian fit in red. Every spectrum has been acquired in the same conditions of previous compounds.

In the case of the Sm(III) compound, the luminescence is again centered around 590 nm. In contrast, the emission spectrum is considerably broadened, $\text{FWHM} = 130$ nm is estimated from Figure 7c. Similar broadenings are found for the Tb(III) and Dy(III) compounds (see Figure 7d,e), presenting $\text{FWHM} = 110$ nm in both cases. This broadening could be explained by variations on the charge environment (with respect to the case of Gd(III) or Er(III) compounds). However, this phenomenon usually comes with a redshift when produced by interaction with the crystal lattice, in contrast, a slight blue shift is observed in the spectra of Tb(III) and Dy(III) compounds (up to 574 and 579 nm, respectively).

A deeper discussion would require a more accurate study about the sensitization dependence on the electronic structure of the lanthanide ions, which is out of the scope of this work. However, the differences with respect to the ligand crystal emissions are only observed in those compounds with optically active resonances at the visible range, and hence, the lanthanide ions should be playing a role. Here, we propose competition between the ligand and the lanthanide emission during the energy transfer as possible explanation. The ligand luminescence dominates the emission due to its shorter lifetime and higher oscillator strength [51,52]. However, part of the excitation energy is transferred to the lanthanide ion, maintaining certain population on the excited states, if available in the visible. The interaction between ligand and ion carriers will be responsible of broadening by spectral diffusion due to electrical screening. In this situation, we could also expect a weak contribution of the lanthanides to the luminescence. Even hindered by the ligand emission, this contribution could be partially responsible for additional broadening and shifts in the emission wavelength. Finally, the contribution of lanthanide ion emission would be favored by the sensitization mechanisms in the case of Ho(III), making possible the estimation of peaks Ho1 and Ho2 in this particular case.

3. Experimental Section

3.1. Starting Materials

All the reagents were commercially available in analytical grade and used without further purification. The sodium salt of the nitroanilate anion, $\text{Na}_2[\text{C}_6\text{N}_2\text{O}_8]$, was prepared according to literature methods [54].

3.2. Synthesis of $[\text{Sm}_2(\text{C}_6\text{O}_4(\text{NO}_2)_2)_3(\text{H}_2\text{O})_{10}]\cdot 6\text{H}_2\text{O}$ (**1**)

A solution of $\text{Sm}(\text{NO}_3)_3\cdot 6\text{H}_2\text{O}$ (4.4 mg, 0.010 mmol) in methanol (2.5 mL) was added dropwise to an aqueous solution (2.5 mL) containing $\text{Na}_2[\text{C}_6\text{N}_2\text{O}_8]$ (4.1 mg, 0.015 mmol) in a diffusion tube. Deep orange crystals suitable for X-ray structure determination were obtained after 10 weeks. The crystals were filtered, washed with methanol, and air dried.

3.3. Synthesis of $[\text{Ln}_2(\text{C}_6\text{O}_4(\text{NO}_2)_2)_3(\text{H}_2\text{O})_{10}]\cdot 6\text{H}_2\text{O}$, $\text{Ln} = \text{Gd}$ (**2**), Tb (**3**), Dy (**4**), Ho (**5**) and Er (**6**)

Compounds **2–6** were synthesized in the same manner as **1** but using $\text{Gd}(\text{NO}_3)_3\cdot 6\text{H}_2\text{O}$ (4.5 mg, 0.01 mmol) (**2**), $\text{Tb}(\text{NO}_3)_3\cdot 5\text{H}_2\text{O}$ (4.4 mg, 0.01 mmol) (**3**), $\text{Dy}(\text{NO}_3)_3\cdot 5\text{H}_2\text{O}$ (4.4 mg, 0.01 mmol) (**4**), $\text{Ho}(\text{NO}_3)_3\cdot 5\text{H}_2\text{O}$ (4.4 mg, 0.01 mmol) (**5**) and $\text{Er}(\text{NO}_3)_3\cdot 5\text{H}_2\text{O}$ (4.4 mg, 0.01 mmol) (**6**) instead of $\text{Sm}(\text{NO}_3)_3\cdot 6\text{H}_2\text{O}$. After 10 weeks, deep orange crystals, suitable for single crystal X-ray structure determination are formed in the diffusion tube (except for compound **6** where only a crystalline powder could be recovered). The crystals were filtered, washed with methanol, and air dried. Note that in compound **6** the number of crystallization water molecules was assumed to be six based on the water molecules observed in compounds **1–5** with X-ray crystal diffraction.

3.4. Physical Measurements

Magnetic susceptibility measurements were carried out in the temperature range 2–300 K with an applied magnetic field of 0.5 T on polycrystalline samples of compounds **1–6** with a Quantum Design (San Diego, CA, USA) MPMS-XL-5 SQUID susceptometer. The susceptibility data were corrected for the sample holders previously measured using the same conditions and for the diamagnetic contributions of the salt as deduced by using Pascal's constant tables [55].

3.5. Crystallographic Data Collection and Refinement

Suitable single crystals of compounds **1–5** were mounted on glass fibers using a viscous hydrocarbon oil to coat the crystal and then transferred directly to the cold nitrogen stream for data collection. X-ray data were collected at 120 K on a Supernova (Oxfordshire, UK) diffractometer equipped with a graphite-monochromated Enhance (Mo) X-ray Source ($\lambda = 0.71073 \text{ \AA}$). The program CrysAlisPro, Oxford Diffraction Ltd., was used for unit cell determinations and data reduction [56]. Empirical absorption correction was performed using spherical harmonics, implemented in the SCALE3 ABSPACK scaling algorithm. The structures were solved by direct methods and successive Fourier difference syntheses, and refined on F^2 by weighted anisotropic full-matrix least-squares methods using the SHELXTL suite of programs [57]. Non-hydrogen atoms were refined anisotropically and hydrogen atoms were assigned fixed isotropic displacement parameters. Data collection and refinement parameters are given in Table 1. CCDC-1494804 (**1**), CCDC-1494806 (**2**), CCDC-1494807 (**3**), CCDC-1494808 (**4**), and CCDC-1494811 (**5**) contain the supplementary crystallographic data for this paper. These data can be obtained free of charge from The Cambridge Crystallographic Data Center via www.ccdc.cam.ac.uk/data_request/cif.

3.6. Luminescence Measurements

The optical measurements have been carried out by means of scanning confocal microscopy using an excitation light of 405 nm. This technique allows simultaneous analysis of the emission spectra

from a surface of hundreds of square microns in order to obtain an average spectra representative of the scanning area. Although this fact limits the spectral resolution of the set-up it is well suited for semi-quantitative discussion of the optical properties of crystalline materials. Notice that our compounds crystallize with different habits and sometimes the emission strongly depends on the measuring point, making hard the comparison among different samples when comparing isolated points.

4. Conclusions

The combination of the nitroanilato ligand ($[\text{C}_6\text{O}_4(\text{NO}_2)_2]^{2-}$ = dianion of the 3,6-dinitro-2,5-dihydroxo-1,4-dibenzoquinone) with lanthanoid metal ions has led to the synthesis of the first Ln-containing nitroanilato complexes. This series of compounds, formulated as $[\text{Ln}_2(\text{C}_6\text{O}_4(\text{NO}_2)_2)_3(\text{H}_2\text{O})_{10}] \cdot 6\text{H}_2\text{O}$, Ln = Sm (1), Gd (2), Tb (3), Dy (4), Ho (5), and Er (6) show a centro-symmetric dimeric structure with a bridging nitroanilato ligand, one terminal nitroanilato ligand, and five coordinated water molecules on each Ln(III) ion. The coordination environment is tricapped trigonal prismatic in all cases. The bond distances follow the expected decreasing trend as we move forward in the lanthanoid series from Sm to Dy and show an abrupt increase in the Ho(III) derivative that can be attributed to an decrease in the distortion of the coordination environment. The magnetic properties show the expected values and behaviors for the corresponding isolated or almost isolated Ln(III) ions and show for the first time that the nitroanilato ligand gives rise to weak magnetic couplings. These compounds show luminescence properties with contributions from the nitroanilato ligand and eventually from the Ln(III) ions, opening the door to a fine tuning of these properties by simply using other anilato-derivative ligands. This work is in progress in our group. We are also performing the synthesis using different metal to ligand ratios in order to obtain coordination complexes and polymers with different dimensionalities and stoichiometries as 1:1 and 1:2, besides the 2:3 observed in compounds 1–6.

Supplementary Materials: The following are available online at www.mdpi.com/2312-7481/2/3/32/s1, Figure S1: Powder X-ray diffractograms of compounds 1–6 compared with the simulated one from the single crystal X-ray structure of compound 5, Table S1: Intermolecular H-bonds with $\text{O} \cdots \text{O}$ distances (in Å) below 2.9 Å involving at least one coordinated or crystallization water molecule for compounds $[\text{Ln}_2(\text{C}_6\text{O}_4(\text{NO}_2)_2)_3(\text{H}_2\text{O})_{10}] \cdot 6\text{H}_2\text{O}$ with Ln = Sm (1), Gd (2), Tb (3), Dy (4), and Ho (5).

Acknowledgments: We thank the Generalitat Valenciana (projects PrometeoII/2014/076 and ISIC) and the Spanish MINECO (project CTQ2014-52758-P) for financial support.

Author Contributions: S.B. designed the synthesis and performed the single crystal and powder X-ray structural analysis. G.L.-M. performed the synthesis of all the compounds. G.L.-M. and J.C.-F. performed the luminescence measurements. C.J.G.-G. performed the magnetic measurements. All the authors contributed to the writing of the manuscript.

Conflicts of Interest: The authors declare no conflict of interest.

References

1. Atzori, M.; Benmansour, S.; Mínguez Espallargas, G.; Clemente-León, M.; Abhervé, A.; Gómez-Claramunt, P.; Coronado, E.; Artizzu, F.; Sessini, E.; Deplano, P.; et al. A Family of Layered Chiral Porous Magnets Exhibiting Tunable Ordering Temperatures. *Inorg. Chem.* **2013**, *52*, 10031–10040. [[CrossRef](#)] [[PubMed](#)]
2. Weng, D.; Wang, Z.; Gao, S. Framework-Structured Weak Ferromagnets. *Chem. Soc. Rev.* **2011**, *40*, 3157–3181. [[CrossRef](#)] [[PubMed](#)]
3. Huang, Y.; Jiang, F.; Hong, M. Magnetic lanthanide–transition-Metal organic–inorganic Hybrid Materials: From Discrete Clusters to Extended Frameworks. *Coord. Chem. Rev.* **2009**, *253*, 2814–2834. [[CrossRef](#)]
4. Givaja, G.; Amo-Ochoa, P.; Gómez-García, C.J.; Zamora, F. Electrical Conductive Coordination Polymers. *Chem. Soc. Rev.* **2012**, *41*, 115–147. [[CrossRef](#)] [[PubMed](#)]
5. Rocha, J.; Carlos, L.D.; Paz, F.A.A.; Ananias, D. Luminescent Multifunctional Lanthanides-Based Metal-Organic Frameworks. *Chem. Soc. Rev.* **2011**, *40*, 926–940. [[CrossRef](#)] [[PubMed](#)]

6. Allendorf, M.D.; Bauer, C.A.; Bhakta, R.K.; Houk, R.J.T. Luminescent Metal-Organic Frameworks. *Chem. Soc. Rev.* **2009**, *38*, 1330–1352. [[CrossRef](#)] [[PubMed](#)]
7. Coronado, E.; Galán-Mascarós, J.R.; Gómez-García, C.J.; Laukhin, V. Coexistence of Ferromagnetism and Metallic Conductivity in a Molecule-Based Layered Compound. *Nature* **2000**, *408*, 447–449. [[CrossRef](#)] [[PubMed](#)]
8. Graham, A.W.; Kurmoo, M.; Day, P. β'' -(bedt-ttf)₄[(H₂O)Fe(C₂O₄)₃]·PhCN: The First Molecular Superconductor Containing Paramagnetic Metal Ions. *J. Chem. Soc. Chem. Commun.* **1995**, *20*, 2061–2062. [[CrossRef](#)]
9. Coronado, E.; Gómez-García, C.J.; Nuez, A.; Romero, F.M.; Waerenborgh, J.C. Synthesis, Chirality, and Magnetic Properties of Bimetallic Cyanide-Bridged Two-Dimensional Ferromagnets. *Chem. Mater.* **2006**, *18*, 2670–2681. [[CrossRef](#)]
10. Coronado, E.; Gómez-García, C.J.; Nuez, A.; Romero, F.M.; Rusanov, E.; Stoeckli-Evans, H. Ferromagnetism and Chirality in Two-Dimensional Cyanide-Bridged Bimetallic Compounds. *Inorg. Chem.* **2002**, *41*, 4615–4617. [[CrossRef](#)] [[PubMed](#)]
11. Kurmoo, M. Magnetic Metal-Organic Frameworks. *Chem. Soc. Rev.* **2009**, *38*, 1353–1379. [[CrossRef](#)] [[PubMed](#)]
12. Newton, G.N.; Nihei, M.; Oshio, H. Cyanide-Bridged Molecular Squares: The Building Units of Prussian Blue. *Eur. J. Inorg. Chem.* **2011**, *2011*, 3031–3042. [[CrossRef](#)]
13. Biswas, S.; Gómez-García, C.J.; Clemente-Juan, J.M.; Benmansour, S.; Ghosh, A. Supramolecular 2D/3D Isomerism in a Compound Containing Heterometallic Cu^{II}₂Co^{II} Nodes and Dicyanamide Bridges. *Inorg. Chem.* **2014**, *53*, 2441–2449. [[CrossRef](#)] [[PubMed](#)]
14. Turner, D.R.; Chesman, A.S.R.; Murray, K.S.; Deacon, G.B.; Batten, S.R. The Chemistry and Complexes of Small Cyano Anions. *Chem. Commun.* **2011**, *47*, 10189–10210. [[CrossRef](#)] [[PubMed](#)]
15. Batten, S.R.; Murray, K.S. Structure and Magnetism of Coordination Polymers Containing Dicyanamide and Tricyanomethanide. *Coord. Chem. Rev.* **2003**, *246*, 103–130. [[CrossRef](#)]
16. Bhowmik, P.; Biswas, S.; Chattopadhyay, S.; Diaz, C.; Gómez-García, C.J.; Ghosh, A. Synthesis, Crystal Structure and Magnetic Properties of Two Alternating Double $\mu_{1,1}$ and $\mu_{1,3}$ Azido Bridged Cu(II) and Ni(II) Chains. *Dalton Trans.* **2014**, *43*, 12414–12421. [[CrossRef](#)] [[PubMed](#)]
17. Adhikary, C.; Koner, S. Structural and Magnetic Studies on Copper(II) Azido Complexes. *Coord. Chem. Rev.* **2010**, *254*, 2933–2958. [[CrossRef](#)]
18. Escuer, A.; Aromí, G. Azide as a Bridging Ligand and Magnetic Coupler in Transition Metal Clusters. *Eur. J. Inorg. Chem.* **2006**, *2006*, 4721–4736. [[CrossRef](#)]
19. Escuer, A.; Esteban, J.; Perlepes, S.P.; Stamatatos, T.C. The Bridging Azido Ligand as a Central Player in High-Nuclearity 3d-Metal Cluster Chemistry. *Coord. Chem. Rev.* **2014**, *275*, 87–129. [[CrossRef](#)]
20. Gu, Z.; Zuo, J.; You, X. A Three-Dimensional Ferromagnet Based on Linked Copper-Azido Clusters. *Dalton Trans.* **2007**, 4067–4072. [[CrossRef](#)] [[PubMed](#)]
21. Tamaki, H.; Zhong, Z.J.; Matsumoto, N.; Kida, S.; Koikawa, M.; Achiwa, N.; Hashimoto, Y.; Okawa, H. Design of Metal-Complex Magnets. Syntheses and Magnetic Properties of Mixed-Metal Assemblies {NBu₄[MCr(ox)₃]}_x (NBu₄⁺ = Tetra(n-Butyl)Ammonium Ion; ox²⁻ = Oxalate Ion; M = Mn²⁺, Fe²⁺, Co²⁺, Ni²⁺, Cu²⁺, Zn²⁺). *J. Am. Chem. Soc.* **1992**, *114*, 6974–6979. [[CrossRef](#)]
22. Kumar, G.; Gupta, R. Molecularly Designed Architectures—The Metalloligand Way. *Chem. Soc. Rev.* **2013**, *42*, 9403–9453. [[CrossRef](#)] [[PubMed](#)]
23. Das, L.K.; Gómez-García, C.J.; Drew, M.G.B.; Ghosh, A. Playing with Different Metalloligands [NiL] and Hg to [NiL] Ratios to Tune the Nuclearity of Ni(II)–Hg(II) Complexes: Formation of Di-, Tri-, Hexa- and Nona-Nuclear Ni–Hg Clusters. *Polyhedron* **2015**, *87*, 311–320. [[CrossRef](#)]
24. Das, L.K.; Gómez-García, C.; Ghosh, A. Influence of the Central Metal Ion in Controlling the Self-Assembly and Magnetic Properties of 2D Coordination Polymers Derived from [(NiL)₂M]²⁺ Nodes (M = Ni, Zn and Cd) (H₂L = Salen-Type Di-Schiff Base) and Dicyanamide Spacers. *Dalton Trans.* **2015**, *44*, 1292–1302. [[CrossRef](#)] [[PubMed](#)]
25. Kitagawa, S.; Kawata, S. Coordination Compounds of 1,4-Dihydroxybenzoquinone and its Homologues. Structures and Properties. *Coord. Chem. Rev.* **2002**, *224*, 11–34. [[CrossRef](#)]
26. Ishikawa, N.; Sugita, M.; Ishikawa, T.; Koshihara, S.Y.; Kaizu, Y. Lanthanide Double-Decker Complexes Functioning as Magnets at the Single-Molecular Level. *J. Am. Chem. Soc.* **2003**, *125*, 8694–8695. [[CrossRef](#)] [[PubMed](#)]

27. Benelli, C.; Gatteschi, D. Magnetism of Lanthanides in Molecular Materials with Transition-Metal Ions and Organic Radicals. *Chem. Rev.* **2002**, *102*, 2369–2387. [[CrossRef](#)] [[PubMed](#)]
28. Roy, L.E.; Hughbanks, T. Magnetic Coupling in Dinuclear Gd Complexes. *J. Am. Chem. Soc.* **2006**, *128*, 568–575. [[CrossRef](#)] [[PubMed](#)]
29. Sessoli, R.; Gatteschi, D.; Caneschi, A.; Novak, M. Magnetic Bistability in a Metal-Ion Cluster. *Nature* **1993**, *365*, 141–143. [[CrossRef](#)]
30. Armelao, L.; Quici, S.; Barigelletti, F.; Accorsi, G.; Bottaro, G. Design of Luminescent Lanthanide Complexes: From Molecules to Highly Efficient Photo-Emitting Materials. *Coord. Chem. Rev.* **2010**, *254*, 487–505. [[CrossRef](#)]
31. Guillou, O.; Daignebonne, C.; Calvez, G.; Bernot, K. A Long Journey in Lanthanide Chemistry: From Fundamental Crystallogenesis Studies to Commercial Anticounterfeiting Taggants. *Acc. Chem. Res.* **2016**, *49*, 844–856. [[CrossRef](#)] [[PubMed](#)]
32. Li, B.; Wen, H.; Cui, Y.; Qian, G.; Chen, B. Multifunctional Lanthanide Coordination Polymers. *Prog. Polym. Sci.* **2015**, *48*, 40–84. [[CrossRef](#)]
33. Bünzli, J.G. On the Design of Highly Luminescent Lanthanide Complexes. *Coord. Chem. Rev.* **2015**, *293–294*, 19–47. [[CrossRef](#)]
34. Song, X.; Song, S.; Zhang, H. (Eds.) Luminescent Lanthanide Metal–Organic Frameworks. In *Lanthanide Metal–Organic Frameworks*; Springer-Verlag: Heidelberg, Germany, 2014; pp. 109–144.
35. Binnemans, K. Interpretation of Europium(III) Spectra. *Coord. Chem. Rev.* **2015**, *295*, 1–45. [[CrossRef](#)]
36. Bünzli, J.C.; Piguet, C. Taking Advantage of Luminescent Lanthanide Ions. *Chem. Soc. Rev.* **2005**, *34*, 1048–1077. [[CrossRef](#)] [[PubMed](#)]
37. Moore, E.G.; Samuel, A.P.; Raymond, K.N. From Antenna to Assay: Lessons Learned in Lanthanide Luminescence. *Acc. Chem. Res.* **2009**, *42*, 542–552. [[CrossRef](#)] [[PubMed](#)]
38. Wu, J.; Zhang, H.; Du, S. Tunable Luminescence and White Light Emission of Mixed lanthanide–organic Frameworks Based on Polycarboxylate Ligands. *J. Mater. Chem. C* **2016**, *4*, 3364–3374. [[CrossRef](#)]
39. Uh, H.; Petoud, S. Novel Antennae for the Sensitization of Near Infrared Luminescent Lanthanide Cations. *C. R. Chim.* **2010**, *13*, 668–680. [[CrossRef](#)]
40. Abrahams, B.F.; Coleiro, J.; Ha, K.; Hoskins, B.F.; Orchard, S.D.; Robson, R. Dihydroxybenzoquinone and Chloranilic Acid Derivatives of Rare Earth Metals. *J. Chem. Soc. Dalton Trans.* **2002**, 1586–1594. [[CrossRef](#)]
41. Benmansour, S.; Gómez-García, C.J. A Heterobimetallic Anionic 3,6-Connected 2D Coordination Polymer Based on Nitroanilate as Ligand. *Polymers* **2016**, *8*, 89. [[CrossRef](#)]
42. Bock, H.; Nick, S.; Nather, C.; Bats, J. Structures of Charge-Perturbed Molecules. 47 Disodium and Dipotassium Nitrates—the Cyanine Distorsion of the Six-Membered Carbon Ring. *Z. Naturforsch. B Chem. Sci.* **1994**, *49*, 1021–1030. [[CrossRef](#)]
43. Robl, C. Complexes with Substituted 2,5-Dihydroxy-Para-Benzoquinones $\text{Ca}[\text{C}_6(\text{NO}_2)_2\text{O}_4] \cdot 4\text{H}_2\text{O}$, $\text{Sr}[\text{C}_6(\text{NO}_2)_2\text{O}_4] \cdot 4\text{H}_2\text{O}$. *Z. Naturforsch. B Chem. Sci.* **1987**, *42*, 972–976.
44. Robl, C.; Weiss, A. Complexes with Substituted 2,5-Dihydroxy-Para-Benzochinones $\text{ZnC}_6(\text{NO}_2)_2\text{O}_4 \cdot 2\text{H}_2\text{O}$. *Z. Naturforsch. B Chem. Sci.* **1986**, *41*, 1337–1340. [[CrossRef](#)]
45. Cotton, F.A.; Murillo, C.A.; Villagran, D.; Yu, R. Uniquely Strong Electronic Communication between $[\text{Mo}_2]$ Units Linked by Dioxolene Dianions. *J. Am. Chem. Soc.* **2006**, *128*, 3281–3290. [[CrossRef](#)] [[PubMed](#)]
46. Kabir, M.; Kawahara, M.; Adachi, K.; Kawata, S.; Ishii, T. One-Dimensional Manganese Assembled Compounds of Bromanilic Acid and Nitranyllic Acid. *Mol. Cryst. Liq. Cryst.* **2002**, *376*, 65–70. [[CrossRef](#)]
47. Benmansour, S.; Gómez-Claramunt, P.; Vallés-García, C.; Mínguez Espallargas, G.; Gómez García, C.J. Key Role of the Cation in the Crystallization of Chiral Tris(Anilato)Metalate Magnetic Anions. *Cryst. Growth Des.* **2016**, *16*, 518–526. [[CrossRef](#)]
48. Benmansour, S.; Vallés-García, C.; Gómez-Claramunt, P.; Mínguez Espallargas, G.; Gómez-García, C.J. 2D and 3D Anilato-Based Heterometallic M(I)M(III) Lattices: The Missing Link. *Inorg. Chem.* **2015**, *54*, 5410–5418. [[CrossRef](#)] [[PubMed](#)]
49. Jhu, Z.; Yang, C.; Lee, G. Two New Series of Rare-Earth Organic Frameworks Involving Two Structural Architectures: Syntheses, Structures and Magnetic Properties. *CrystEngComm* **2013**, *15*, 2456–2465. [[CrossRef](#)]
50. Sorace, L.; Gatteschi, D. Electronic Structure and Magnetic Properties of Lanthanide Molecular Complexes. In *Lanthanide and Actinides in Molecular Magnetism*; Layfield, R.A., Murugesu, M., Eds.; Wiley-VCH Verlag GmbH & Co. KGaA: Weinheim, Germany, 2015; Volume 1, pp. 1–25.

51. Szostak, M.M.; Kozankiewicz, B.; Lipinski, J. Low-Temperature Photoluminescence of p-Nitroaniline and o-Methyl-p-Nitroaniline Crystals. *Spectrochim. Acta A Mol. Biomol. Spectrosc.* **2007**, *67*, 1412–1416. [[CrossRef](#)] [[PubMed](#)]
52. Malinowski, M.; Frukacz, Z.; Szuflińska, M.; Wnuk, A.; Kaczkan, M. Optical Transitions of Ho₃ in YAG. *J. Alloys Compd.* **2000**, *300–301*, 389–394. [[CrossRef](#)]
53. Liu, L.; Zhang, N.; Leng, Z.; Liang, Y.; Li, R.; Zou, L.; Gan, S. Highly bright multicolour emission through energy migration in core/shell Nanotubes. *Dalton Trans.* **2015**, *44*, 6645–6654. [[CrossRef](#)] [[PubMed](#)]
54. Huang, Y.; Gao, H.; Twamley, B.; Shreeve, J.M. Highly Dense Nitranilates-Containing Nitrogen-Rich Cations. *Chem. Eur. J.* **2009**, *15*, 917–923. [[CrossRef](#)] [[PubMed](#)]
55. Bain, G.A.; Berry, J.F. Diamagnetic Corrections and Pascal's Constants. *J. Chem. Educ.* **2008**, *85*, 532–536. [[CrossRef](#)]
56. *CrysAlisPro*, Version 171.33.55. Oxford Diffraction Ltd.: Oxforshire, UK, 2004.
57. Sheldrick, G.M. A Short History of SHELX. *Acta Cryst. A* **2008**, *64*, 112–122. [[CrossRef](#)] [[PubMed](#)]



© 2016 by the authors; licensee MDPI, Basel, Switzerland. This article is an open access article distributed under the terms and conditions of the Creative Commons Attribution (CC-BY) license (<http://creativecommons.org/licenses/by/4.0/>).